Langmuir

Article

pubs.acs.org/Langmuir

New Insight into the Stability of $CaCO_3$ Surfaces and Nanoparticles via Molecular Simulation

A. Matthew Bano,[†] P. Mark Rodger,[†] and David Quigley*[,‡]

[†]Department of Chemistry and Centre for Scientific Computing, University of Warwick, Coventry CV4 7AL, U.K.

[‡]Department of Physics and Centre for Scientific Computing, University of Warwick, Coventry CV4 7AL, U.K.

ABSTRACT: Using updated and improved atomistic models for the polymorphs of calcium carbonate and their constituent ions in solution, we revisit the question of surface energetics and nanoparticle stability. Using a simple lattice-based Monte Carlo scheme, we generate nanoparticle configurations in vacuum for all three biologically relevant polymorphs of calcium carbonate and establish that the bulk energetic ordering of polymorphs persists to the nanoscale. In aqueous environments, results based on surface enthalpy alone indicate that formation of mineral−water interfaces is marginally favorable in many cases. Including an estimate of lost entropy due to formation of structured water layers is sufficient to reverse this observation, implying a delicate balance of enthalpy and entropy at crystalline $CaCO_3$. In contradiction to some previous studies, we find that small calcite nanoparticles with diameters in the range of 1.8−4.1 nm do not retain an ordered structure on nanosecond time scales. The consequences of these results for simulation studies of biomineralization are discussed.

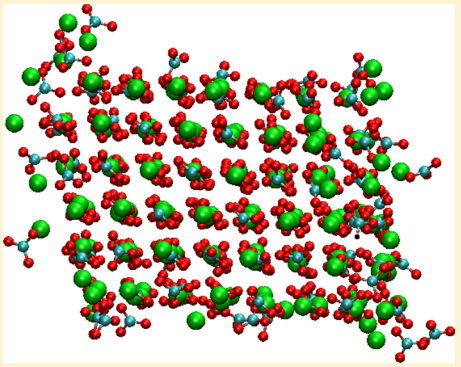

INTRODUCTION

Calcium carbonate ($CaCO_3$) is a common biomineral, exploited by nature for the formation of a variety of structures required by organisms for defense, structural support, or other purposes. A diverse range of mechanisms are exploited to grow structures that exhibit order over a hierarchy of length scales, leading to desirable material properties beyond those possessed by single crystals of the component mineral. These mechanisms can involve prenucleation clusters,[1,2] dense liquid precursor phases,[3] growth via metastable polymorphs,[4] and assembly of nanoparticles into larger structures.[5] Each of these stages may be controlled, moderated, or directed by the presence of organic scaffolds, proteins, and other biomolecules in the growth environment.[6]

The early stages of these processes are not directly accessible to experiment, and hence, significant effort has been expended to develop atomic scale models and simulation protocols to capture the essential ingredients of these nonclassical crystal nucleation and growth pathways.[7−16] In recent years, a new family of $CaCO_3$ models have been developed[17−19] focused on correctly capturing the energetics of all relevant crystalline phases, and the statistical thermodynamics of ions in solution relative to them. Most notably, solvation free energies of both Ca^{2+} and CO_3^{2-} have been fit via thermodynamic perturbation methods, requiring extensive sampling with molecular dynamics.

In this paper, we explicitly study the energetics of the $CaCO_3$ crystal−water interface in light of these improved models. These newer atomistic models correct several deficiencies of those used in earlier studies, generally fit only to readily computable static properties of one or two crystal polymorphs, such as lattice parameters, elastic constants, and vibrational mode frequencies. There have also been inconsistencies in how one older model in particular has been applied in the literature. The potential of Pavese et al.[20,21] is fit to the calcite and aragonite structures, the most stable polymorphs under biologically relevant conditions. Both polymorphs retain their experimental symmetry groups upon relaxation with this model, only if a particular choice of exclusion rules is applied to intramolecular C−O and O−O interactions.[22] However, to reproduce the lattice energies reported by De Leeuw and Parker[23] in their survey of $CaCO_3$ surface energies, one must use different exclusion rules;[24] their use causes aragonite to relax to a lower-symmetry structure via in-plane rotation of carbonate ions.

Previous work by Cooke and Elliott[25] has used the well-known Wulff construction, within the same model used by De Leeuw and Parker,[23] to generate atomistic representations of calcite nanoparticles in both vacuum and aqueous environments. Perhaps surprisingly, the observed effect of water solvent was to stabilize order within these particles, such that nanocrystals as small as 18 formula units remained ordered after simulation for tens of nanoseconds. No aragonite or vaterite particles were constructed or simulated.

A particular aim of this work is to study the energetics of both calcite and aragonite surfaces and to study the relative energetics of calcite, aragonite, and vaterite nanoparticles. This extends the studies described above and also provides

Received: April 14, 2014
Revised: June 9, 2014
Published: June 10, 2014

   dx.doi.org/10.1021/la501409j | *Langmuir* 2014, 30, 7513−7521

important thermodynamic data against which to interpret simulations of crystal growth. We stress from the outset that our adoption of newer atomistic models is likely to lead to conclusions qualitatively different from those observed in previous simulation studies. In particular, the calcite dissolution energetics of many of the older models have been demonstrated to be in error by an order of magnitude and a sign.[17] Furthermore, only the most recent model correctly captures the difference in sign between the dissolution enthalpy and the dissolution free energy of calcite, signifying the importance of entropic contributions in determining the qualitative behavior of the $CaCO_3$–water system.

The remainder of this paper is structured as follows. We first construct nanocrystals of the three relevant calcium carbonate polymorphs in a vacuum environment and present a simple alternative to the standard Wulff construction. The relative energetics of these polymorphs are compared as a function of particle size. Next we study the energetics of mineral–water interfaces for calcite and aragonite. Finally, we simulate a selection of crystalline nanoparticles explicitly in an aqueous environment.

NANOPARTICLES IN A VACUUM

Wulff Constructions. In common with De Leeuw and Parker,[23] we first compute surface energies in vacuum and use these to generate low-energy nanoparticle configurations via the Wulff construction. We stress that the Wulff construction has a number of limitations, both conceptual and practical. When applied to nanoscale crystallites, the approximation of interfacial energetics with those computed from ideal infinite planar surfaces is likely to be overly aggressive. Indeed, the effect of edge and corner energetics could very well dominate. Furthermore, upon construction of an atomistic representation of the resulting idealized morphology, one is restricted to "magic numbers" of ions that satisfy the constraints of the crystal structure, charge neutrality, and idealized morphology. Nevertheless, Wulff-constructed particles are a useful starting point and allow us to make direct comparisons with previous work.

Vacuum surface energies were computed for both calcite and aragonite using GULP,[26] and we refer the reader to the Supporting Information of ref 19 for details about the model and its parameters. In each case, surfaces were constructed parallel to each of the 25 planes with the smallest interplanar spacing, these being expected to exhibit the lowest energies.[27] Surface configurations were generated using GDIS,[28] retaining all lattice shifts corresponding to terminations of the bulk lattice at an atomic layer. The mineral slab was divided into two regions, with the upper layer free to relax while the lower layer is held fixed. Periodic boundary conditions are applied in directions perpendicular to the surface normal. The energies of these surface configurations were converged with respect to the depth of both regions. In all cases, the upper region was at least 10 Å thick and the lower layer at least 8 Å. The surface energy was computed per unit area of surface by comparison with bulk lattice energies at the same pressure.

As expected, for calcite, only the $\{10\bar{1}4\}$ surface is expressed. This differs only slightly from the earlier work of De Leeuw and Parker, in which a small facet of $\{10\bar{1}1\}$ appears in the Wulff morphology.[23] More recent calculations by Roberto et al.[29,30] using the potential of Rohl et al.[31] express a number of additional surfaces, with a significantly smaller energetic difference between the facets involved. For example, in our work, the second most stable surfaces are computed as $\{10\bar{1}0\}$, being 0.33 J mol^{-1} higher in energy than the $\{10\bar{1}4\}$ set. This is similar to the value of 0.38 J mol^{-1} computed by De Leeuw and Parker[23] using the Pavese model, but rather larger than the 0.19 J mol^{-1} difference computed by Roberto et al. with the Rohl et al. model, explaining the dramatic different in equilibrium morphology.

The computed energy of the calcite $(10\bar{1}4)$ surface[32] is given in Table 1, in comparison with those of the 10 lowest-energy aragonite surfaces obtained. The precision shown is that to which the computed surface energies converge with respect to the two surface region depths. We note that the energy of the calcite $(10\bar{1}4)$ surface is lower than that of any obtained for aragonite, suggesting that surface effects alone cannot (in vacuum) offset the bulk energetic preference for calcite. We stress that these are relaxed surface energies but acknowledge that relaxation to a local minimum may not yield the lowest-energy structure for a given surface. We are not aware of any known surface reconstruction of aragonite relevant at biological temperatures.

Table 1. Ten Lowest-Energy Surfaces Computed for Aragonite with a Calcite $(10\bar{1}4)$ Surface for Comparison

aragonite surface	shift	surface energy (J m^{-2})
(011)	0.50	0.8406
(102)	0.00	0.8780
(112)	0.50	0.8955
(102)	0.50	0.9358
(001)	0.00	1.0161
(110)	0.50	1.0350
(012)	0.00	1.0848
(221)	0.50	1.1041
(122)	0.00	1.1068
(013)	0.00	1.1115
(012)	0.50	1.1136
(010)	0.00	1.1467
(211)	0.25	1.1662
calcite surface	shift	surface energy (J m^{-2})
$(10\bar{1}4)$	0.00	0.7113

Applying the Wulff constructions to these surface energies, we recover the expected rhombohedral equilibrium morphology for calcite. The computed aragonite equilibrium morphology is shown in Figure 1. This does not express all of the surfaces present in the experimental morphology, which is dominated by {011}, {110}, and {010} faces. The vacuum morphology computed by De Leeuw and Parker does express the {110} and {011} surfaces, but not in the correct morphology, despite the failure of the model to correctly capture the bulk aragonite crystal structure. Note that in the

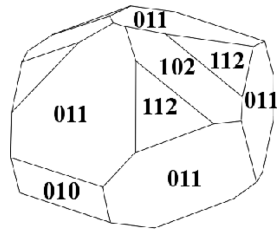

Figure 1. Computed vacuum Wulff construction morphology for aragonite.

dx.doi.org/10.1021/la501409j | Langmuir 2014, 30, 7513–7521

current context, we do not expect vacuum surface enthalpies to lead to morphologies that are consistent with experimentally grown aragonite crystals, as the energetics of the water−aragonite interaction are likely to be highly significant in this model.

Ion Site Monte Carlo. Two factors motivate us to seek options for generating nanocrystal morphologies beyond those provided by the Wulff construction. First, because of the aforementioned magic number effects, we are able to generate only six atomistic representations of our aragonite morphology for particle sizes between 80 and 180 $CaCO_3$ units, this being the range of interest for comparison with previous metadynamics calculations (using an older model potential).[9,15] Second, we also hope to construct vaterite particles, for which computation of representative bulk-terminated surfaces is problematic because of orientational disorder in the carbonate sublattice.[33] De Leeuw and Parker avoided this issue by using a fully ordered supercell of vatertite,[34] in which all three possible orientation positions are present in the correct ratio, to construct their surfaces. An alternative ordered vaterite structure is that of Wang and Becker,[35] which can be considered as the lowest-energy (within the present model) realization of orientational disorder. It is not clear if surfaces generated with any of these ordered structures are representative of those generated by cleaving the partially disordered crystal, particularly as the energy required to interconvert between realizations of the disorder is comparable to the thermal energy at room temperature.

We propose a simple but effective method for generating atomistic representations of nanoparticles in vacuum. We begin with a representation of the bulk lattice, large enough such that the required nanoparticle size can be carved from its interior. Lattice sites are then randomly populated, such that the total number of $CaCO_3$ formula units matches that in the required nanoparticle. We then perform Metropolis Monte Carlo (MMC) moves in which pairs of lattice site occupancies are randomly swapped until the system reaches a stable low-energy configuration. The temperature used in the MMC algorithm should be considered an optimization parameter and is not physically meaningful. In principle, low-energy sets of lattice occupancies will correspond to nanoparticles.

As ions only ever occupy ideal lattice site positions, all intramolecular CO_3^{2-} interactions can be neglected, and intermolecular interactions can be tabulated for efficiency. The algorithm is, however, very slow to converge. To rectify this, we implement a configurational bias scheme, which enhances the probability of attempting to swap the occupancies of lattice sites that are at the boundary of the evolving nanoparticle, by preferentially selecting those with small numbers of occupied neighbors. Detailed balance is maintained by modifying the acceptance probability for occupancy swaps accordingly. We refer to this method of generating particle configurations as ion site Monte Carlo (ISMC).

In the case of vaterite, the bulk lattice sites for ISMC are those of Kamhi,[33] retaining all three possible orientations at each CO_3^{2-} center, allowing a treatment of disorder to be implemented naturally by MMC moves that select an orientation at random and imposing the constraint that only a single orientation at each carbonate site can be occupied. Note the use of this structure is appropriate within the presently employed model potential, where realizations of this disorder are true energetic minima. However, recent first-principles calculations by Demichelis et al.[36,37] have shown that many ordered candidate structures for vaterite are in fact transition states between five lower-energy vaterite structures. We retain an explicit treatment of disorder in our calculations.

This method imposes no morphology constraint, allowing us to generate nanoparticles containing an arbitrary number of formula units. For calcite, the method recovers the expected $\{10\bar{1}4\}$ dominated rhombohedra (matching the Wulff construction exactly) upon application at sizes commensurate with the Wulff magic numbers. At other sizes, rhombohedra exhibiting steps are obtained. Such configurations may prove to be useful for future studies of morphology control, where biological molecules may bind preferentially at the step edge. For aragonite, we typically generate nanoparticles somewhat different from the Wulff construction described above, most notably omitting the {001} and {210} surfaces, suggesting that corner and edge energies involving these faces are significant for particles of this size *in vacuo*. In solvent, such features may be stabilized, recovering the expected equilibrium shape. Example particles generated from all three polymorphs are shown in Figure 2.

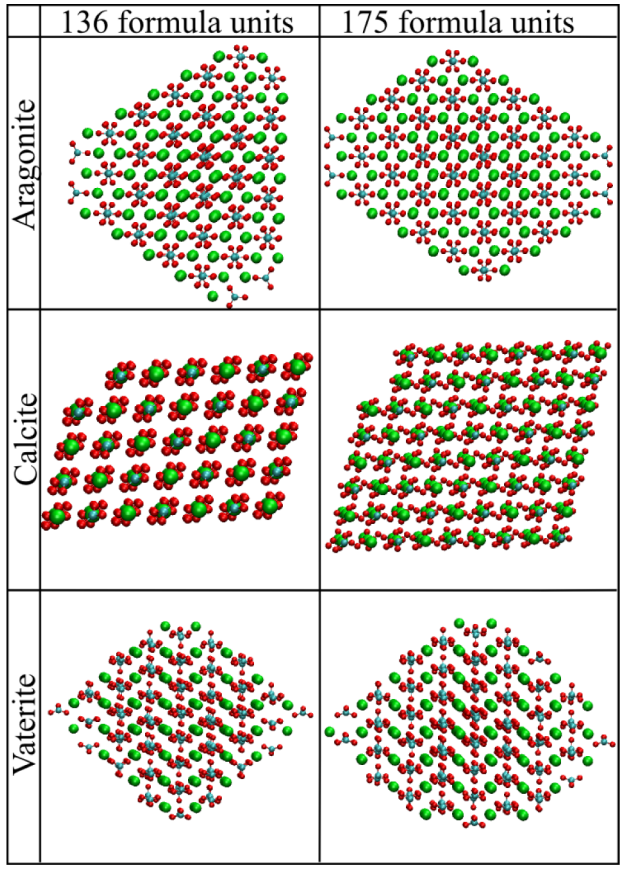

Figure 2. Example nanoparticles generated via the ISMC technique for each of the three polymorphs: calcite, aragonite, and vaterite.

Relaxed and unrelaxed energies for each polymorph at particle sizes between 80 and 180 formula units are shown in Figure 3. Upon relaxation, all ISMC aragonite particles have energies equal to or lower than those of the Wulff-constructed equivalents. While it is somewhat disingenuous to interpret these results in the context of nanoparticle growth from solution, we can make a few general observations. First, the energetic ordering of polymorphs does not change as a function of particle size over the range considered. This indicates (at

dx.doi.org/10.1021/la501409j | *Langmuir* 2014, 30, 7513−7521

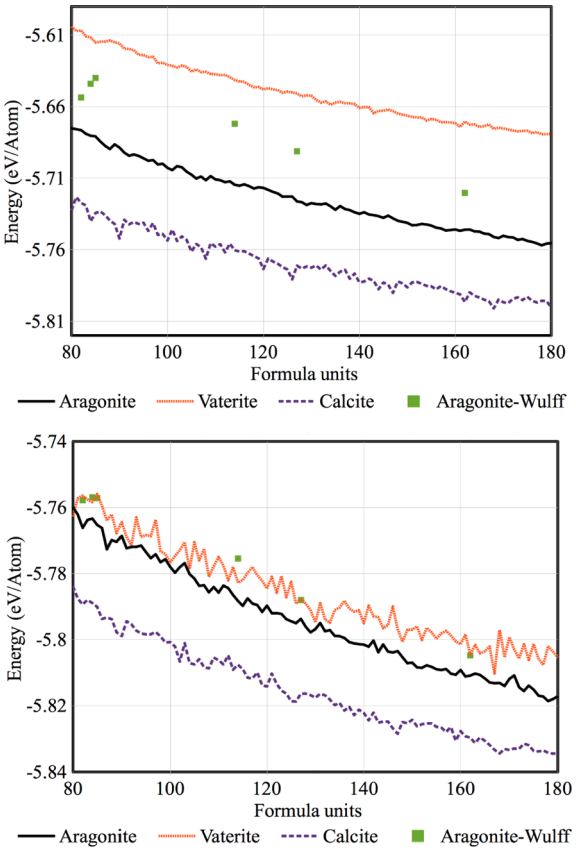

Figure 3. Unrelaxed (top) and relaxed (bottom) energies of calcium carbonate nanoparticles generated using ISMC for the three relevant polymorphs of calcium carbonate. In the case of aragonite, the energies of Wulff-constructed nanoparticles are shown for comparison.

least in vacuum) that surface effects are not capable of offsetting the bulk energetic ordering, even at the nanoscale. However, there are particle sizes at which the energetic difference between aragonite and vaterite is extremely small, suggesting that transformation from vaterite precursor particles directly to aragonite may be achievable with thermal energy, provided the hydration energies of these two nanocrystals are comparable.

CRYSTAL–WATER INTERFACES

We now turn our attention to the more relevant question of hydrated surfaces and nanoparticles. In principle, the quantity of interest when comparing the stability of various mineral surfaces is interfacial free energy γ, defined as the cost per unit area of creating a mineral–water interface. In simulation terms

$$\gamma_{hkl} = \left(G_{hkl}^{\mathrm{min-wat}} - N_{\mathrm{CaCO_3}} g^{\mathrm{min}} - N_{\mathrm{H_2O}} g^{\mathrm{wat}}\right) / \left(2A_{hkl}^{\mathrm{min-wat}}\right) \quad (1)$$

where the first term on the right-hand side of eq 1 is the Gibbs free energy evaluated in a periodic simulation cell containing two equivalent interfaces between the mineral crystal and water, containing $N_{\mathrm{CaCO_3}}$ formula units of the mineral and $N_{\mathrm{H_2O}}$ water molecules, constructed such that the interface between the two lies parallel to the plane (hkl) and is of area $A_{hkl}^{\mathrm{min-wat}}$. The specific Gibbs free energies per formula unit of mineral and water in bulk are denoted g^{min} and g^{wat}, respectively. Well-established methods exist for accurately computing the free energies of the two bulk phases, for example, by thermodynamic integration along a reversible path connecting the system to a reference state of known free energy, typically the ideal gas for fluid phases, and the Einstein crystal for solids. Evaluating the free energy of the interfacial system is problematic. The cleaving method of Broughton and Gilmer[38] can construct a reversible path between two bulk unit cells and the interfacial system. However, with the exception of the ice–water interface,[39] it has yet to be applied beyond systems modeled with simple pair potentials.[40,41]

Hence, upon comparison of the energetics of solvated mineral surfaces, it is common to approximate γ by the surface enthalpy, replacing the free energies in eq 1 with enthalpies, and hence neglecting any entropic contribution to the cost of forming the interface in question. In the case of calcite, there is reason to doubt the validity of this approximation. As reported by a number of authors,[25,42] the calcite–water interface exhibits a number of layers of structured water at the surface. The immobilization of these molecules constitutes a reduction in entropy, which has yet to be quantified explicitly. Nevertheless, we begin our investigation of hydrated surface energetics by computing surface enthalpies only.

Enthalpies for the two bulk phases, and for the simulation cells containing mineral–water interfaces, were computed by averaging samples over molecular dynamics simulations (>1 ns) at 300 K and 1 atm of pressure. The angles defining the shape of the simulation box were constrained, but the dimensions were allowed to vary independently to sample at the required pressure.

All trajectories were computed with LAMMPS[43] and were subject to an initial equilibration period of 0.25 ns. For each interface considered, care was taken to converge the surface enthalpy with respect to the thickness of the water and mineral layers perpendicular to the interface. An example simulation cell is shown in Figure 4. In all cases, the mineral layer was at least

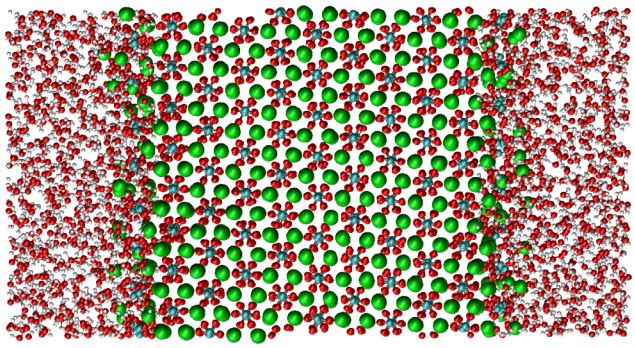

Figure 4. Example aragonite surface simulation cell. In this case, the (110) surface is exposed to the water layer. At this and many other aragonite surfaces, the mineral–water interface is diffuse and requires simulation for several nanoseconds to yield equilibrated energetics.

40 Å thick, with the water layer no thinner than 30 Å. The water model used is the SPC/Fw model of Wu et al.,[44] and we again refer the reader to ref 19 for details of the water–mineral interaction.

Computed surface enthalpies for a representative sample of the aragonite surfaces studied are shown in Figure 5, along with the associated statistical uncertainty. Although small in magnitude, many of these surface enthalpies are negative. If these data were accurate approximations for the interfacial free energy densities for aragonite surfaces, then one would expect bulk crystals to be unstable in aqueous environments, spontaneously breaking up to form crystal–water interfaces.

dx.doi.org/10.1021/la501409j | Langmuir 2014, 30, 7513–7521

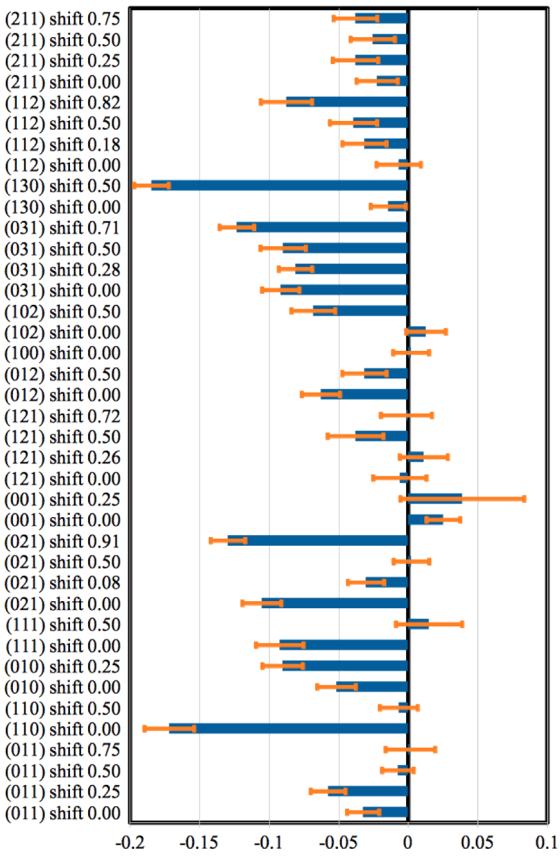

Figure 5. Computed interfacial enthalpies in joules per square meter for a selection of aragonite surfaces, simulated at 300 K and 1 atm of pressure, over equilibrium trajectories of >1 ns. Orange bars denote the statistical standard error.

We find the structuring of water at many of these aragonite surfaces to be comparable to that on the calcite $(10\bar{1}4)$ surface. Our computed value for the calcite $(10\bar{1}4)$ surface enthalpy is -0.010 ± 0.015 J m^{-2}, i.e., also negative, but with a magnitude smaller than the statistical uncertainty in our calculations. For crystallites to be stable, all surface energies must be positive. Our results therefore require that the missing entropic contribution to γ be positive, corresponding to a loss of entropy upon formation of a crystal–water interface, and larger in magnitude than the surface enthalpy.

We defer attempts to compute the entropic contribution accurately for future work; however, it is instructive to make an estimate of its magnitude for comparison with data in Figure 5. Such an estimate can be obtained by approximating the structured water at the mineral interface as icelike, whereupon the entropy lost per unit area in immobilizing a sheet of surface water can be computed from the entropy of fusion in the ice–liquid water system. In the case of a 5 Å thick layer, which is conservative for many of the surfaces simulated, this leads to a correction $(-T\Delta S)$ of $\approx$0.17 J m^{-2} at 300 K. It is therefore not unreasonable to suggest that this entropic penalty can compensate for the negative surface enthalpy, being of the same order of magnitude but having the opposite sign.

It is instructive to compare our calcite hydrated $(10\bar{1}4)$ surface enthalpy at 300 K to surface energies obtained with continuum solvation models. Two recent studies have used the COSMIC[45] method to compute energies of static, hydrated $(10\bar{1}4)$ surfaces. Bruno et al.[30] computed a value of 0.49 J m^{-2}. Estimates of the vibrational contribution to the interfacial energy are combined with a measurement of the calcite–water contact angle to obtain (via Young's relation) an estimate of the interfacial free energy of 0.41 J m^{-2} at 300 K. More recently, Heberling et al.[46] have use improved solvation parameters (and the same interatomic potential used in the study presented here) to obtain a value of 0.26 J m^{-2} for the interfacial energy. Following the same procedure as Bruno et al., this reduces to 0.18 J m^{-2} for the interfacial free energy, which is very close to our figure when including the approximate correction for lost entropy mentioned above.

NANOPARTICLES IN WATER

Without accurate calculations of the surface free energy, it is not sensible to use our computed hydrated surface data to generate meaningful Wulff constructions for aragonite. Furthermore, these would be relevant only to very large crystallites in which well-developed facets have emerged and the effect of corner, edge, and step energies is limited.

We therefore complement the calculations described above with a study of stability and structural order in small nanoparticles embedded in explicit solvent. Particle sizes ranging from 75 to 256 formula units (diameter from ≈1.8 to 4.1 nm) were studied over 12 ns simulations.

In each case, ISMC-constructed nanocrystals were immersed in a cubic simulation cell containing enough water molecules to effectively screen interactions across the periodic boundaries. This criterion requires between 7200 and 8100 water molecules depending on the particle size. We note that such simulations are often considered an effective representation of an infinitely dilute suspension of nanoparticles. However, in the limit of long time scales, one would expect such simulations to exhibit partial dissolution of ions from the nanocrystal to establish equilibrium with a saturated solution, i.e., the concentration of $CaCO_3$ in the surrounding solution should be finite at equilibrium.

In practice, our use of a nonreactive force field for the water solvent effectively restricts us to simulations in the high-pH limit, where the solubility of calcite reaches its minimum. The saturated solution equilibrium in this limit would represent only a handful of dissolved ions in even our largest simulation cells. The time scales required to reach such an equilibrium are likely to be prohibitive. Indeed, we are aware of only a single attempt by Aragones et al.[47] to fully equilibrate a system of solute (in this case an NaCl crystal) in contact with a saturated solvent, using molecular dynamics. A downward trend in the energy could still be observed after simulation for several microseconds, implying that even longer times would be required to fully equilibrate the system. It is therefore unsurprising that our simulations do not reach equilibrium, as indicated by plots in Figure 6 of enthalpy versus simulation time, for 90 and 147 $CaCO_3$ units. However, in several of our simulations, there is clear evidence of dissolution from the corners of the nanoparticles, as indicated in Figure 7. This effect was entirely absent from previous studies[25] and should be considered a desirable consequence of correctly capturing solution energetics in the newer generation of $CaCO_3$ models.

Despite an inability to reach equilibrium with a saturated solution, we find it instructive to quantify the amount of crystalline order remaining in each of our nanoparticles following the 12 ns simulation. In the work of Cooke and Elliott, the presence of an ordered calcite structure within solvated nanoparticles was quantified using an order parameter

dx.doi.org/10.1021/la501409j | Langmuir 2014, 30, 7513–7521

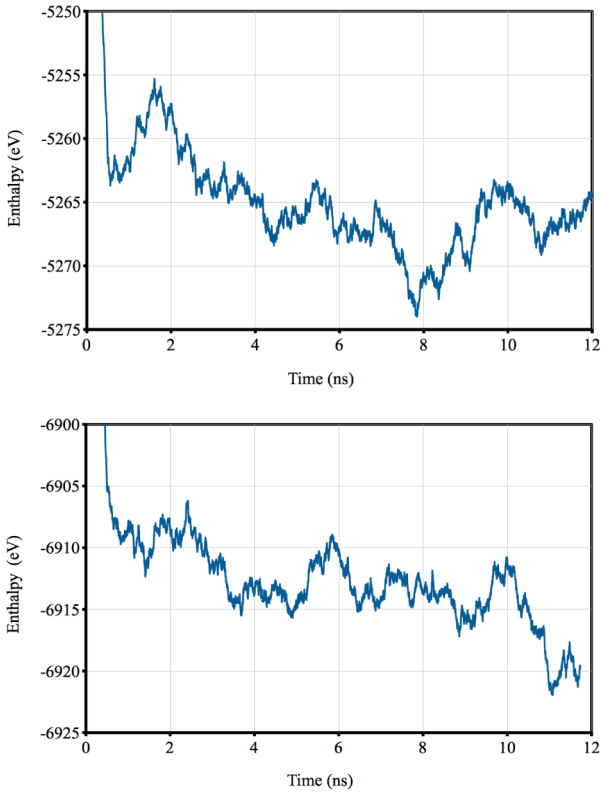

Figure 6. Enthalpy vs simulation time for two example simulations of calcite nanoparticles immersed in water. The top panel corresponds to 90 formula units of $CaCO_3$ and the bottom panel to 147 formula units. Neither simulation has reached a stable equilibrium with the surrounding solvent.

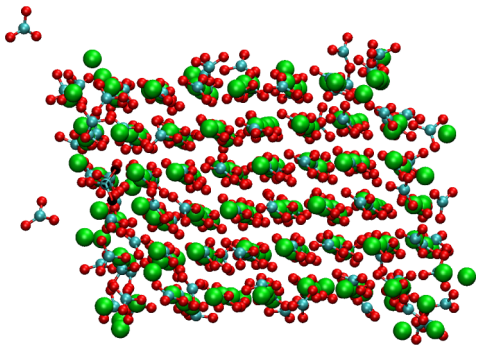

Figure 7. Example simulation snapshot after simulation for 12 ns for a 192 formula unit calcite nanoparticle in water. Dissolution of ions from the corners of the nanocrystal is evident. The surrounding water solvent is hidden for the sake of clarity.

based on the mean rotation of carbonate groups from their initial (ideal) position. Here we adopt a graph theoretic approach to measure order, closely based on that previously used by Hobbs et al.[48] to study the topology of silica networks. Representing atoms as vertices on a graph, we first construct edges from calcium vertices to any carbon vertices located within a spherical cutoff of 4.7 Å. Within this network representation, one can identify all primitive rings that pass through a given atom and hence define a local cluster comprising all the vertices involved in these rings.

Table 2 lists the number of vertices and four- and six-membered rings (which we collectively term "primitive ring statistics") for local clusters constructed around calcium and

Table 2. Local Cluster Statistics for Calcium Carbonate Polymorphs

local cluster	no. of vertices	no. of four-membered rings	no. of six-membered rings
calcite Ca	27	12	24
calcite C	27	12	24
aragonite Ca	31	12	42
aragonite C	39	12	42
vaterite Ca	39	12	42
vaterite C	31	12	42

carbon sites in the three polymorphs of $CaCO_3$ of interest in this study. Each local cluster is illustrated in Figure 8. The

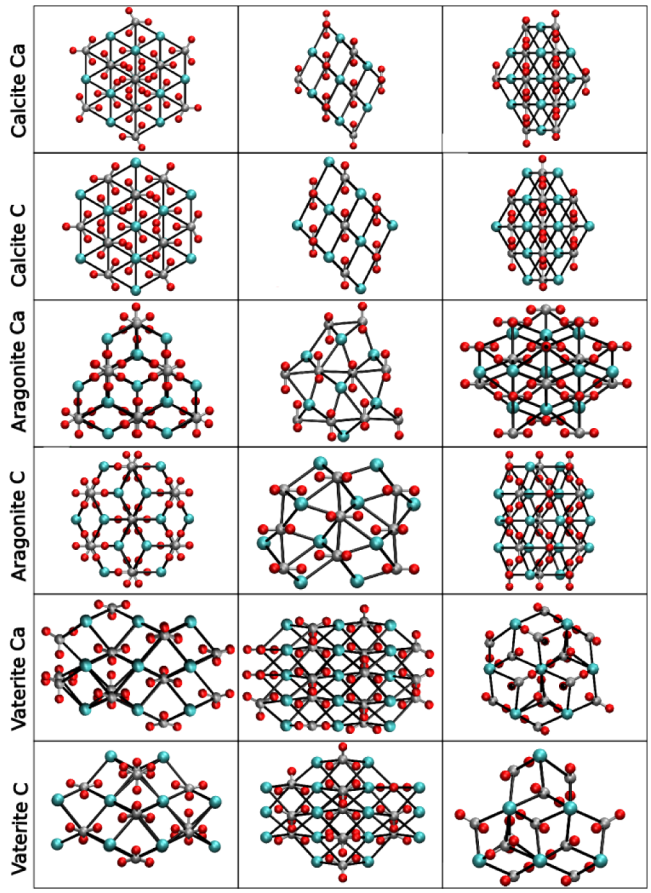

Figure 8. Projections of local clusters within the three polymorphs of calcium carbonate. The definition of local cluster is insensitive to the orientation of the carbonate ion and is hence equivalent for all realizations of vaterite disorder. Calcium ions are represented as blue spheres, carbon atoms as gray spheres, and oxygen atoms as red spheres.

values in Table 2 can be used as a fingerprint to identify individual Ca ions that are in an environment consistent with each given polymorph. The primitive ring statistics can be calculated for each ion within an arbitrary cluster, and those ions for which the number of vertices and rings exactly matches the values for one of the polymorphs can be identified with that polymorph. In this way, it is possible to calculate a polymorph composition for each cluster. Although this method is more difficult to implement than the method described in ref 15, we find this topological approach to be less sensitive to distortions of the crystal lattice in the particle subsurface and hence able to

dx.doi.org/10.1021/la501409j | Langmuir 2014, 30, 7513−7521

identify a greater number of ions with bulk polymorphs. Nevertheless, we are unable to assign ions <4.7 Å from a particle boundary to a bulk polymorph, because of termination of the primitive rings at surfaces.

Using this analysis, we define the residual order within a nanoparticle to be the number of e.g. calcite-like ions remaining at the end of the simulation divided by the number identified within the initial, ideal nanoparticle. A scatter plot of residual order versus nanoparticle size is shown in Figure 9. There is a

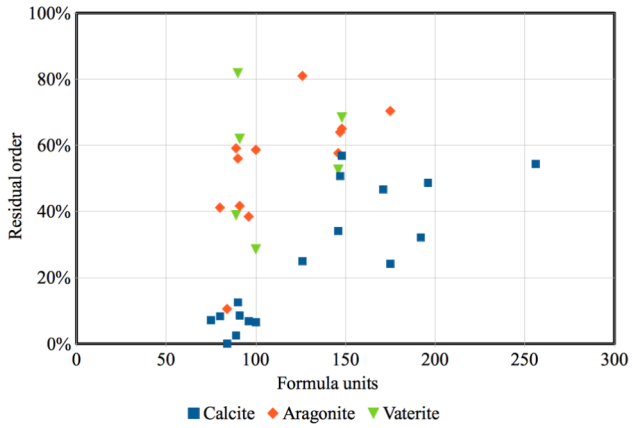

Figure 9. Residual order identified via primitive ring statistics following simulation for 12 ns in water for various nanoparticle sizes and initial structures.

clear trend for increased residual order with particle size for calcite. For comparison, we also plot the residual (aragonite-like) order for ISMC nanoparticles constructed for aragonite in vacuum, stressing that we do not expect the resulting morphology to be representative of real solvated aragonite nanocrystals. Here the trend is less clear, but generally aragonite particles retain more of their initial order on this time scale than calcite particles. Partial dissolution is also observed, but it is not possible on this time scale to determine if the models correctly capture the higher solubility of aragonite with respect to calcite.

The loss of nearly all crystalline order for small particles is entirely consistent with previous free energy calculations by Raiteri and Gale,[18] which indicate a clear preference for amorphous structure in nanoparticles up to approximately 3 nm in diameter. Crystalline nanoparticles become energetically competitive at larger sizes but still do not dominate even at the largest studied diameter (4.5 nm).

DISCUSSION

Any atomistic simulation of crystal growth must be interpreted within the context of the model used. In the case of biomineral nucleation and growth, a key part of this context is mineral–water interfacial thermodynamics. Unlike ionic solvation free energies, it is not yet possible to build interfacial free energies directly into a model fitting process or even to calculate them routinely given an existing model. In this work, we have demonstrated that recent models, fitted to capture the thermodynamic of bulk phases and of ions in solution, lead to a delicate balance of surface enthalpy and entropy at the mineral–water interface.

We stress that our conclusion is not that mineral–water surface enthalpies are negative, but rather that these are sufficiently small for the enthalpic and entropic contributions to be in delicate balance. This is a familiar situation from other questions of stability in $CaCO_3$. The free energy of dissolution for calcite is roughly equal in magnitude but opposite in sign to the dissolution enthalpy, and purely enthalpic calculations erroneously suggest that aragonite is the most stable crystal polymorph. One may argue that such small surface enthalpies are unlikely to be correctly captured by simple atomistic models. Indeed, there is evidence that the current model has room for improvement in its description of the calcite–water interface.[49] *Ab initio* data (not without limitation) are available for comparison.[50] Nevertheless, this model matches experimentally determined dissolution and ion solvation energetics to within a few percent,[17] an order of magnitude improvement on older models. Hence, we do not expect further refinements to alter our conclusion with regard to the magnitude of energetic quantities.

Our data can be used to suggest new insight into the ease with which nature is able to control crystal morphology and preferentially select metastable polymorphs during growth. For example, several marine organisms readily grow aragonite crystallites under conditions where calcite is the thermodynamically stable bulk phase. One can argue that under these circumstances, small crystallites of aragonite may be stabilized by a interfacial free energy with the surrounding solvent lower than that of calcite, offsetting the bulk preference by virtue of a large surface area to volume ratio. Our results dictate that this situation can arise entirely via small differences in the entropic contribution to that interfacial free energy and cannot arise from purely enthalpic considerations.

This leads us to suggest that the action of biological polymorph/morphology control may also be completely entropic, resulting from disruption or enhancement of the interfacial water structure by biomolecules. This can be accomplished without any need for biomolecules to bind strongly (or at all) to the mineral surface itself and is an appealing alternative to more complex arguments based on kinetic control.

We have also demonstrated that it is possible to simulate directly the early stages of nanoparticle dissolution, toward equilibrium with a saturated solution, although reaching that equilibrium within an achievable simulation time is still unattainable. Furthermore, we have demonstrated that hydrated nanocrystals of calcite smaller than ∼4 nm spontaneously amorphise on <20 ns time scales.

These observations present a number of challenges to future simulations probing the influence of biomolecules on the $CaCO_3$ nucleation and growth process. Simulations of proteins or peptides interacting with even the smallest stable calcite nanocrystal would need to be significantly larger than any reported to date. Attempts to quantify the thermodynamic influence of these molecules on surface stability should also include entropic contributions due to disruption of the strongly bound water layer, demonstrated by our data to be far from negligible. Accurately quantifying these contributions will require further advances in calculation methodology.

AUTHOR INFORMATION

Corresponding Author

*E-mail: d.quigley@warwick.ac.uk.

Notes

The authors declare no competing financial interest.

dx.doi.org/10.1021/la501409j | *Langmuir* 2014, 30, 7513–7521

■ ACKNOWLEDGMENTS

Computing facilities were provided by the Centre for Scientific Computing at the University of Warwick and by the HECToR service. D.Q. is grateful for the award of an EPSRC Career Acceleration Fellowship (EP/H00341X/1). A.M.B. was supported by an EPSRC Doctoral Training grant (EP/F500378/1). Further support was provided via EPSRC Grant EP/I001514/1.

■ REFERENCES

(1) Gebauer, D.; Voelkel, A.; Coelfen, H. Stable Prenucleation Calcium Carbonate Clusters. *Science* **2008**, *322*, 1819−1822.
(2) Pouget, E. M.; Bomans, P. H. H.; Goos, J. A. C. M.; Frederik, P. M.; de With, G.; Sommerdijk, N. A. J. M. The Initial Stages of Template-Controlled $CaCO_3$ Formation Revealed by Cryo-TEM. *Science* **2009**, *323*, 1455−1458.
(3) Wallace, A. F.; Hedges, L. O.; Fernandez-Martinez, A.; Raiteri, P.; Gale, J. D.; Waychunas, G. A.; Whitelam, S.; Banfield, J. F.; De Yoreo, J. J. Microscopic Evidence for Liquid-Liquid Separation in Supersaturated $CaCO_3$ Solutions. *Science* **2013**, *341*, 885−889.
(4) Ihli, J.; Wong, W. C.; Noel, E. H.; Kim, Y.-Y.; Kulak, A. N.; Christenson, H. K.; Duer, M. J.; Meldrum, F. C. Dehydration and crystallization of amorphous calcium carbonate in solution and in air. *Nat. Commun.* **2014**, *5*, 3169.
(5) Coelfen, H.; Antonietti, M. Mesocrystals: Inorganic Superstructures Made by Highly Parallel Crystallization and Controlled Alignment. *Angew. Chem., Int. Ed.* **2005**, *44*, 5576−5591.
(6) Chen, C.-L.; Qi, J.; Zuckermann, R. N.; DeYoreo, J. J. Engineered Biomimetic Polymers as Tunable Agents for Controlling $CaCO_3$ mineralization. *J. Am. Chem. Soc.* **2011**, *133*, 5214−5217.
(7) Bulo, R. E.; Donadio, D.; Laio, A.; Molnar, F.; Rieger, J.; Parrinello, M. Site Binding of Ca^{2+} Ions to Polyacrylates in Water: A Molecular Dynamics Study of Coiling and Aggregation. *Macromolecules* **2007**, *40*, 3437−3442.
(8) Harding, J. H.; Duffy, D. M.; Sushko, M. L.; Rodger, P. M.; Quigley, D.; Elliott, J. A. Computational Techniques at the Organic-Inorganic Interface in Biomineralization. *Chem. Rev.* **2008**, *108*, 4823−4854.
(9) Quigley, D.; Rodger, P. M. Free energy and structure of calcium carbonate nanoparticles during early stages of crystallization. *J. Chem. Phys.* **2008**, *128*, 221101.
(10) Quigley, D.; Rodger, P. M. A metadynamics-based approach to sampling crystallisation events. *Mol. Simul.* **2009**, *35*, 613−623.
(11) Tribello, G. A.; Bruneval, F.; Liew, C.; Parrinello, M. A Molecular Dynamics Study of the Early Stages of Calcium Carbonate Growth. *J. Phys. Chem. B* **2009**, *113*, 11680−11687.
(12) Tribello, G. A.; Liew, C.; Parrinello, M. Binding of Calcium and Carbonate to Polyacrylates. *J. Phys. Chem. B* **2009**, *113*, 7081−7085.
(13) Quigley, D.; Rodger, P. M.; Freeman, C. L.; Harding, J. H.; Duffy, D. M. Metadynamics simulations of calcite crystallization on self-assembled monolayers. *J. Chem. Phys.* **2009**, *131*, 094703.
(14) Freeman, C.; Harding, J.; Quigley, D.; Rodger, P. Structural Control of Crystal Nuclei by an Eggshell Protein. *Angew. Chem., Int. Ed.* **2010**, *49*, 5135−5137.
(15) Quigley, D.; Freeman, C. L.; Harding, J. H.; Rodger, P. M. Sampling the structure of calcium carbonate nanoparticles with metadynamics. *J. Chem. Phys.* **2011**, *134*, 044703.
(16) Freeman, C. L.; Harding, J. H.; Quigley, D.; Rodger, P. M. Protein binding on stepped calcite surfaces: Simulations of ovocleidin-17 on calcite 31.16 and 31.8. *Phys. Chem. Chem. Phys.* **2012**, *14*, 7287−7295.
(17) Raiteri, P.; Gale, J. D.; Quigley, D.; Rodger, P. M. Derivation of an Accurate Force-Field for Simulating the Growth of Calcium Carbonate from Aqueous Solution: A New Model for the Calcite-Water Interface. *J. Phys. Chem. C* **2010**, *114*, 5997−6010.
(18) Raiteri, P.; Gale, J. D. Water Is the Key to Nonclassical Nucleation of Amorphous Calcium Carbonate. *J. Am. Chem. Soc.* **2010**, *132*, 17623−17634.
(19) Demichelis, R.; Raiteri, P.; Gale, J. D.; Quigley, D.; Gebauer, D. Stable prenucleation mineral clusters are liquid-like ionic polymers. *Nat. Commun.* **2011**, *2*, 590.
(20) Pavese, A.; Catti, M.; Parker, S. C.; Wall, A. Modelling of the thermal dependence of structural and elastic properties of calcite, $CaCO_3$. *Phys. Chem. Miner.* **1995**, *23*, 89−93.
(21) Pavese, A.; Catti, M.; Price, G. D.; Jackson, R. A. Interatomic potentials for $CaCO_3$ polymorphs (calcite and aragonite), fitted to elastic and vibrational data. *Phys. Chem. Miner.* **1992**, *19*, 80−87.
(22) In this case, excluding only intramolecular carbon−oxygen Coulomb interactions, but retaining all oxygen−oxygen interactions.
(23) De Leeuw, N. H.; Parker, S. C. Surface Structure and Morphology of Calcium Carbonate Polymorphs Calcite, Aragonite, and Vaterite: An Atomistic Approach. *J. Phys. Chem. B* **1998**, *102*, 2914−2922.
(24) We are only able to reproduce the reported energies when no intramolecular Coulomb interactions are excluded.
(25) Cooke, D. J.; Elliott, J. A. Atomistic simulations of calcite nanoparticles and their interaction with water. *J. Chem. Phys.* **2007**, *127*, 104705.
(26) Gale, J. D.; Rohl, A. L. The General Utility Lattice Program (GULP). *Mol. Simul.* **2003**, *29*, 291−341.
(27) Donnay, J. D. H.; Harker, D. A new law of crystal morphology extending the Law of Bravais. *Am. Mineral.* **1937**, *22*, 446−467.
(28) Fleming, S.; Rohl, A. GDIS: A visualization program for molecular and periodic systems. *Z. Kristallogr.* **2005**, *220*, 580−584.
(29) Roberto, M. F.; Marco, B.; Dino, A. Effect of the Surface Relaxation on the Theoretical Equilibrium Shape of Calcite. 1. The [001] Zone. *Cryst. Growth Des.* **2010**, *10*, 4096−4100.
(30) Bruno, M.; Massaro, F. R.; Pastero, L.; Costa, E.; Rubbo, M.; Prencipe, M.; Aquilano, D. New Estimates of the Free Energy of Calcite/Water Interfaces for Evaluating the Equilibrium Shape and Nucleation Mechanisms. *Cryst. Growth Des.* **2013**, *13*, 1170−1179.
(31) Rohl, A. L.; Wright, K.; Gale, J. D. Evidence from surface phonons for the (2 × 1) reconstruction of the (10-14) surface of calcite from computer simulation. *Am. Mineral.* **2003**, *88*, 921−925.
(32) Our computed value is consistent with the value if 0.71 J mol^{-1} reported in ref 46 using the same model potential.
(33) Kamhi, S. R. On the structure of vaterite, $CaCO_3$. *Acta Crystallogr.* **1963**, *16*, 770−772.
(34) Meyer, H. J. Struktur und Fehlordnung des Vaterits. *Z. Kristallogr.* **1969**, *128*, 183−212.
(35) Wang, J.; Becker, U. Structure and carbonate orientation of vaterite ($CaCO_3$). *Am. Mineral.* **2009**, *94*, 380−386.
(36) Demichelis, R.; Raiteri, P.; Gale, J. D.; Dovesi, R. A new structural model for disorder in vaterite from first-principles calculations. *CrystEngComm* **2012**, *14*, 44−47.
(37) Demichelis, R.; Raiteri, P.; Gale, J. D.; Dovesi, R. The Multiple Structures of Vaterite. *Cryst. Growth Des.* **2013**, *13*, 2247−2251.
(38) Broughton, J. Q.; Gilmer, G. H. Molecular dynamics investigation of the crystal-fluid interface. VI. Excess surface free energies of crystal-liquid systems. *J. Chem. Phys.* **1986**, *84*, 5759−5768.
(39) Handel, R.; Davidchack, R. L.; Anwar, J.; Brukhno, A. Direct Calculation of Solid-Liquid Interfacial Free Energy for Molecular Systems: TIP4P Ice-Water Interface. *Phys. Rev. Lett.* **2008**, *100*, 036104.
(40) Davidchack, R. L.; Laird, B. B. Simulation of the hard-sphere crystal−melt interface. *J. Chem. Phys.* **1998**, *108*, 9452−9462.
(41) Davidchack, R. L.; Laird, B. B. Direct Calculation of the Hard-Sphere Crystal/Melt Interfacial Free Energy. *Phys. Rev. Lett.* **2000**, *85*, 4751−4754.
(42) Kerisit, S.; Cooke, D.; Spagnoli, D.; Parker, S. Molecular dynamics simulations of the interactions between water and inorganic solids. *J. Mater. Chem.* **2005**, *15*, 1454−1462.
(43) Plimpton, S. Fast Parallel Algorithms for Short-Range Molecular Dynamics. *J. Comput. Phys.* **1995**, *117*, 1−19.
(44) Wu, Y.; Tepper, H. L.; Voth, G. A. Flexible simple point-charge water model with improved liquid-state properties. *J. Chem. Phys.* **2006**, *124*, 024503.

(45) Gale, J. D.; Rohl, A. L. An efficient technique for the prediction of solvent-dependent morphology: The COSMIC method. *Mol. Simul.* **2007**, *33*, 1237−1246.
(46) Heberling, F.; Vinograd, V. L.; Polly, R.; Gale, J. D.; Heck, S.; Rothe, J.; Bosbach, D.; Geckeis, H.; Winkler, B. A thermodynamic adsorption/entrapment model for selenium(IV) coprecipitation with calcite. *Geochim. Cosmochim. Acta* **2014**, *134*, 16−38.
(47) Aragones, J. L.; Sanz, E.; Vega, C. Solubility of NaCl in water by molecular simulation revisited. *J. Chem. Phys.* **2012**, *136*, 244508.
(48) Hobbs, L. W.; Jesurum, C. E.; Pulim, V.; Berger, B. Local topology of silica networks. *Philos. Mag. A* **1998**, *78*, 679−711.
(49) Fenter, P.; Kerisit, S.; Raiteri, P.; Gale, J. D. Is the Calcite−Water Interface Understood? Direct Comparisons of Molecular Dynamics Simulations with Specular X-ray Reflectivity Data. *J. Phys. Chem. C* **2013**, *117*, 5028−5042.
(50) Villegas-Jimenez, A.; Mucci, A.; Whitehead, M. A. Theoretical Insights into the Hydrated (10.4) Calcite Surface: Structure, Energetics, and Bonding Relationships. *Langmuir* **2009**, *25*, 6813−6824.